Journal of Solid State Chemistry **148,** 250–259 (1999)
Article ID jssc.1999.8446, available online at http://www.idealibrary.com on IDEAL®

New Ternary Compounds $Sc_3B_{0.75}C_3$, $Sc_2B_{1.1}C_{3.2}$, $ScB_{15}C_{1.60}$ and Subsolidus Phase Relations in the Sc–B–C System at 1700°C

Y. Shi, A. Leithe-Jasper, and T. Tanaka[1]

National Institute for Research in Inorganic Materials, Namiki 1-1, Tsukuba, Ibaraki 305-0044, Japan

Received November 4, 1998; in revised form July 8, 1999; accepted July 22, 1999

The phase relations in the ternary system scandium–boron–carbon with special emphasis on the boron-rich section have been investigated in an isothermal section at 1700°C. Ternary compounds with the following stoichiometries were identified: Sc_2BC_2, $Sc_3B_{0.75}C_3$, $Sc_2B_{1.1}C_{3.2}$, ScB_2C_2, $ScB_{17}C_{0.25}$, $ScB_{15}C_{0.80}$, and $ScB_{15}C_{1.60}$. Four of them, $Sc_3B_{0.75}C_3$, $Sc_2B_{1.1}C_{3.2}$, $ScB_{15}C_{1.60}$, and $ScB_{15}C_{0.80}$, were synthesized for the first time. The first three could be indexed, i.e., Sc_3BC_3 shows tetragonal symmetry with $a = 3.3308(3)$ Å and $c = 7.680(2)$ Å; the basic hexagonal unit cell of $Sc_2B_{1.1}C_{3.2}$ is $a = 3.3991(2)$ Å, $c = 6.7140(6)$ Å, with a two-dimensional incommensurate structure with magnitude $|q_i| = (2/7 + 0.005)\ |q_{100}|$ Å^{-1} along ⟨100⟩ directions; and $ScB_{15}C_{1.60}$ shows a body centered orthorhombic lattice $a = 10.027(1)$ Å, $b = 8.0138(9)$ Å and $c = 5.6668(6)$ Å. A crystal of Sc_2BC_2 was grown by the floating zone method and the crystal structure was refined from single crystal data, which crystallizes with tetragonal symmetry: $I4/mmm$, $a = 3.3259(2)$ Å, $c = 10.6741(8)$ Å, $Z = 2$, $R = 0.011$ for 263 unique reflections and 10 variables.

Key Words: **scandium borides; scandium carbides; scandium boron-carbides; phase relations; crystal structure refinement; $Sc_3B_{0.75}C_3$; $Sc_2B_{1.1}C_{3.2}$; $ScB_{15}C_{1.60}$; $ScB_{15}C_{0.80}$; Sc_2BC_2.**

1. INTRODUCTION

Ternary boron–carbides of rare-earth and actinide metals have been the subject of continuous scientific interest with regard to a variety of structures, chemical and physical properties. A few phase diagrams of *R*–B–C systems (*R* = Y(1), Eu(2), Gd(3), and Ho(4)) have been published. (For a recent compilation of metal–boron–carbon systems the reader is referred to Ref. (5).) Except for the recently found boron-rich ternary compound $ScB_{17}C_{0.25}$ (6), several distinct structure types of ternary compounds are at present known to exist (5, 7). The formation of compounds belonging to one of these is strongly correlated with the size of lanthanide elements. The smallest size rare-earth element, scandium, shows some peculiarities in the formation of boron-carbides, such as the formation of the ScB_2C_2 structure type which is not observed for other rare-earth metals in the RB_2C_2 series (8). This suggests the possibility of the formation of hitherto unknown boron-carbide based structures.

Moreover, the unique bonding nature of boron-rich borides enables them to form compounds with very complicated crystal structures and some fascinating properties. YB_{66}, whose crystal structure is a fcc lattice formed by super-icosahedra $(B_{12})_{12}B_{12}$, has been used as a soft X-ray monochromator for synchrotron radiation in the 1 to 2 keV energy region (9). Crystal structures of several new binary rare-earth boron-rich borides, such as YB_{50} (10), YB_{25} (11), and ScB_{19} (12), are also based on bonding between boron icosahedra (B_{12}). Because of the decomposition behavior of the above-mentioned borides, the melt growth method by the addition of a third element has been introduced for single crystal growth. For the YB_{50} phase, the addition of silicon has resulted in successful crystal growth of the isostructural compound $YB_{44}Si_{1.0}$ (13). However, as for the ScB_{19} phase, the addition of carbon resulted in the formation of another novel ternary compound: $ScB_{17}C_{0.25}$ (6). Because YB_{66} has a very low thermal conductivity of 2×10^{-2} W/cm/K at room temperature, it prevents the widespread use of YB_{66} as a monochromator, especially on beam lines with higher X-ray flux. The search for substitute material with higher thermal conductivity is therefore strongly motivated. Except for yttrium and scandium, other rare-earth elements have intrinsic M-absorption edges below 2 keV and their compounds are not usable as a monochromator in this energy region. Thus, the search for new monochromators with superior properties highly motivates this investigation of the ternary Sc–B–C system.

2. EXPERIMENTAL PROCEDURES

2.1. Powder Synthesis

The starting materials were Sc_2O_3 powder (4N, Crystal System Inc., Japan), amorphous boron (3N, SB-Boron Inc.,

[1]To whom correspondence should be addressed. E-mail: tanakat@nirim.go.jp.

0022-4596/99 $30.00

USA), and graphite (3N, Koujundo Kagaku Co., Japan). From them via carbothermal and borothermal reduction reactions precursor materials were synthesized. Choosing Sc_2O_3 powder instead of pure Sc metal as a Sc source to start with facilitates a homogeneous big batch powder metallurgical synthesis especially for boron-rich samples where phase equilibria were found to be rather hampered once the sample was molten. It is also difficult to control the chemical compositions of the samples by arc-melting pure Sc, B, and C elements because the evaporation pressure of Sc is high. Nevertheless, in a very few cases (binary ScC_{1-x} compound) where serious doubts of possible oxygen influence on structural properties existed some samples were also prepared by conventional arc-melting of Sc metal chips with compacted graphite powder in proper stoichiometry under a protective atmosphere of Zr gettered Ar gas. These molten samples were then annealed at about 1700°C in vacuum for at least 10 hours.

Although carbothermal reduction of oxide material may introduce oxygen contamination, the oxygen analyses of nearly all samples synthesized by this method show less than 1 wt.% oxygen impurity. Thus, in most cases scandium borides (only in the boron-rich region) or carbide ScC_{1-x} (another part of the ternary phase diagram) were synthesized. Then the desired amount of carbon and boron were added to the scandium boride or carbide powder. For the synthesis of scandium boride, oxygen can be understood to be lost in the simple form of BO according to the following reaction equation:

$$Sc_2O_3 + (2m + 3)B \rightarrow 2ScB_m + 3BO\uparrow.$$

A carbothermal reduction yields not only CO gas as assumed in Ref. (14). For the synthesis of scandium oxycarbide $Sc_2C_xO_y$, comparing the carbon content before and after reaction, it was found that the final yielding gas should contain both CO and CO_2 with an approximate mole ratio of 2 : 1. This value varied depending on the reaction condition such as the initial chemical composition, heating time, and temperature. The chemical reaction can be described schematically as following:

$$Sc_2O_3 + C \rightarrow Sc_2C_xO_y + [CO\uparrow + CO_2\uparrow].$$

If the $Sc_2C_xO_y$ phase is subsequently annealed by adding small amounts of B (less than 10 at.%), the oxygen impurity can be reduced to less than 1 wt.% in the mixtures of ScC_{1-x} and ScB_2. Using pre-reacted samples ScB_xC_y, such as the starting materials, can avoid oxygen contamination rather effectively.

Stoichiometric mixtures of powders were isostatically pressed into pellets at 250 MPa. The pellet was reacted at about 1700°C in vacuum for at least 10 hours in a boron nitride crucible which was inserted into an inductively heated graphite susceptor. Temperature was measured using an optical pyrometer (0.65 μm) by simulating black body condition through a small drilled hole in the crucible lid. In order to obtain equilibrium, all the samples were crushed, reshaped, and subject to at least a second anneal.

2.2. Single Crystal Growth

The crystal was grown by a floating-zone method in a xenon-lamp image furnace under continuous flow of Ar (99.999 wt.%) gas. Polycrystalline sintered rods of Sc_2BC_2 were used as feed and seed rods. They were prepared by a solid state reaction as described above. Both the feed rod and the growing crystal were synchronously driven downward at a rather low speed of 4 mm/hour under a counter rotation of 30 rpm.

2.3. Characterizations

After the powder was dissolved into a HNO_3 + HCl (1 : 1) solution keeping it at 150°C for 16 hours, the scandium and boron contents were determined by a chelate titration and inductively coupled plasma atomic emission spectroscopy, respectively. The carbon content was determined by a volumetric combustion method using a carbon determinator (WR-12, Leco Co.). Oxygen impurities of ternary compounds were analyzed by a standard inert gas fusion method (TC-136, Leco Co.). As rare-earth borocarbides tend to decompose by moisture in air, only freshly prepared powders were analyzed. Nevertheless, it has to be assumed that during the process of powder preparation for oxygen analysis some amount of oxygen impurities via the oxidation products are additionally incorporated. Lack of chemical analysis data in the literature (usually only metallic impurity levels of starting materials are given) makes comparison of our oxygen levels with other independent investigations impossible.

Phase identification was carried out using a standard X-ray powder diffractometer (R-2000, Rigaku Co.) with Cu$K\alpha$ radiation. The $K\alpha1$ peak intensities were determined after rejecting $K\alpha2$ peaks, using RINT software (Rigaku Co.).

The electron diffraction patterns were derived at an acceleration voltage of 100 kV using a standard transmission electron microscope (Hitachi H-500). The scanning electron microscopy was measured by a Hitachi S-5000.

The X-ray reflections of single crystal data were collected on an Enraf-Nonius CAD4 automatic four-circle diffractometer with graphite monochromated Mo$K\alpha$ radiation. The intensity data were corrected for Lorentz and polarization effects. The absorption correction applied to the collected data was based on a Gaussian numerical integration employing the measured dimension of the single crystal (15).

3. RESULTS AND DISCUSSION

3.1. Phase Relations

3.1.1. Binary Systems

3.1.1.1. The boron–carbon system. The technologically very important boron–carbon system and the binary compound "B_4C" have been the topic of numerous scientific investigations (see Ref. (16) and references therein). A recent assessment (17) of the B–C binary shows congruent melting (2452°C) 'B_4C' with a broad homegeneity range with a stoichiometry of $B_{4.1}C$ at the carbon-rich side and B_9C at the boron-rich one, respectively, which is accepted in this work. The rhombohedral crystal structure of boron carbide consists of icosahedra and C–B–C chains (18, 19). The compositions richer in boron are formed by boron carbon substitution in the icosahedra as well as in the linear chains (20). Interstitial sites and chain center vacancies also play a significant role in forming this remarkably wide range of stoichiometry as well as most likely hosting light atom impurities: e.g., Si, O, Al, etc. (21–23). All these parameters significantly influence the unit cell dimensions observed. This rather complex interplay of local disorder and accommodation of small amounts of impurities makes it difficult to compare literature results since they strongly depend on the method and conditions of synthesis applied (20, 24). The overall trend observed in all scientific contributions shows an increase of the unit cells' dimension with increasing boron content. This is also confirmed in this work.

3.1.1.2. The scandium boron system. Recently it was found that a new boron-rich tetragonal ScB_{19} phase (12) has to be included in the established Sc–B binary (25) which was previously understood to be composed only of congruent melting hexagonal ScB_2 (2250°C), tetragonal ScB_{12} (2040°C), and "ScB_{28}," which represents the maximum solubility of Sc in rhombohedral β-Boron (26). We confirm the existence and structure of these compounds. The structure of ScB_{12} has been the topic of contradicting investigations claiming crystallization in the cubic UB_{12} structure ($a_{cub} = 7.402(3)$ Å) (27) or a tetragonal structure ($a, b = 5.22$, $c = 7.34$ Å) derived from UB_{12} (28). It was found that traces of other rare earth-metals in ScB_{12} can stabilize the cubic structure (29). Our own findings strongly support the tetragonal lattice, although with formation of a complicated superstructure (a, b, c_{sst}) with $a, b_{sst} = a_{cub} * 4/\sqrt{2}$ and $c_{sst} = a_{cub} * 2$ (30).

3.1.1.3. The scandium carbon system. The binary phase diagram of Sc–C was established by (31). It consists of congruent melting of ScC_{1-x}, Sc_4C_3 ("Sc_2C_3"), and Sc_3C_4 ("$Sc_{15}C_{19}$"). Sc_4C_3 is proposed to melt incongruently with a high temperature modification stable between 1864 and 1504°C and a low temperature modification stable down to 950°C. Sc_3C_4 was found to melt incongruently at 1794°C and is stable down to room temperature. ScC_{1-x} has been the topic of several investigations (32–35). It exhibits a considerable range of homogeneity (e.g., at 1700°C, ScC_{1-x} with $0.28 < x < 0.55$). Much attention was paid to the role of oxygen solubility in this substoichiometric compound isotypic with NaCl (34, 36–38). The occurrence of superstructure formation in a sample with $ScC_{0.7}$ stoichiometry (annealed <1350°C) could be contradictingly interpreted on the base of a cubic supercell with doubled lattice parameter (32) or a trigonal structural model similar to Y_2C (35, 39). While Ref. (33) reported the formation of a cubic body centered Sc_2C_3 phase isotypic with Pu_2C_3 (35), based on neutron diffraction data, refined its composition and structure to Sc_4C_3 of anti-Th_3P_4 type. Previously a tentative composition of $Sc_{15}C_{19}$ was assigned for the phase with highest C content in the Sc–C system (40). Nevertheless a recent structure determination (41) of this compound revealed that the correct composition is Sc_3C_4 with unique C_3 units in the tetragonal unit cell as a structural feature.

Our findings confirm the existence and a significant homogeneity range of ScC_{1-x}. In Table 1 we document the dependence of the lattice constant on the carbon content. No indication of a trigonal or cubic superstructure could be found in our samples. We can also find a correlation of the size of the unit cell with an oxygen impurity content. Since it was shown that carbothermically synthesized ScC_{1-x} cannot be obtained oxygen free (38), we synthesized some samples by arc melting Sc metal and graphite. Samples with an oxygen impurity level ≤ 0.5 wt.% clearly show an increase of the unit cell dimension with increasing C content in accordance with Ref. (33). Once the oxygen impurity level exceeds 0.5 wt.% the lattice seems to shrink significantly approaching the value of 4.576(3) Å observed for "Sc_2OC" in a sample containing also Sc_3C_4 (38). Despite the fact that

TABLE 1
Phase Analysis of the ScC_{1-x} Homogeneous Region

	Composition (Chemical analysis at.%)					Lattice parameter of fcc ScC_{1-x}
No.	C			O (wt.%)	Phase identification	(Å)
Binary-1	21.52			0.42	ScC_{1-x} + Sc	4.518(4)
Binary-2	28.11			0.50	Pure ScC_{1-x}	4.655(1)
Binary-3	30.69			0.39	Pure ScC_{1-x}	4.668(2)
Binary-4	34.84			1.01	ScC_{1-x} + Sc_3C_4 (traces)	4.593(5)
Binary-5	39.50			0.98	ScC_{1-x} + Sc_3C_4	4.586(3)
	SC	B	C	O (wt.%)		
Ternary-1[a]	44.24	50.25	5.50	0.063	ScC_{1-x} + ScB_2	4.512(2)
Ternary-2[b]	59.52	13.12	27.36	1.046	ScC_{1-x} + ScB_2	4.578(1)

[a]Ternary-1 was synthesized by the arc-melting method.
[b]Ternary-2 was synthesized by carbothermal reduction.

in our samples the oxygen content is clearly much lower and the carbon content higher than in a Sc_2OC phase the lattice constant seems to be quite insensitive after a certain small amount of oxygen is incorporated into the lattice. The role of oxygen as a structural stabilizing element in Sc(O, C, □) is also strongly backed by band structure calculations (37) indicating the necessity of additional oxygen to form a Sc carbide adopting the NaCl structure.

Sc_4C_3 seems to be unstable at 1700°C since it was never observed in our samples. Nevertheless its pattern could be found in some arc-melted specimens prior to the annealing process. This is in contradiction to the observation in (35) which tended to attribute stability to Sc_4C_3 at temperatures not exceeding 1600°C. We found Sc_3C_4 to exist at 1700°C in accordance with the literature (31, 38).

3.1.2. Ternary System

3.1.2.1. Sc rich (Sc–ScB_2–$B_{4.1}C$) section. In this section of the phase diagram four ternary compounds were identified: $Sc_3B_{0.75}C_3$, $Sc_2B_{1.1}C_{3.2}$, Sc_2BC_2 (42), ScB_2C_2 (44). The first two are novel compounds which will be discussed seperately. It should be mentioned that the compound ScB_2C (43) is only stable at very high temperatures. It could be synthesized by arc-melting but after annealing at 1700°C for more than 20 hours it decomposes to ScB_2 and ScB_2C_2. The other two known ternary compounds synthesized under our experimental conditions showed consistent lattice parameters with the reported data. No indications of homogeneic regions were found. Figure 1 presents the phase equilibria as observed at 1700°C. Table 2 lists the chemical analysis results and phase identifications of some representative samples whose positions are also denoted in Fig. 1. Similar to other rare-earth diborides (4) ScB_2 exhibits significant carbon solubility indicated by change of the unit cell's dimensions. This lattice parameter variation (see Table 2) can be explained by small amounts of carbon substitute for boron atoms in the hexagonal rings in the *a–b* plane of the ScB_2 (AlB_2 type structure), which decrease the bond length of these hexagonal rings. This results in a decrease of the *a* parameter and subsequently the *c* parameter increases. Due to the significant evaporation losses (a similar observation was made in Ref. (45) in their study of the evaporation characteristics of ScB_2) no attempt to quantify the exact amount of dissolved C in ScB_2 was successful and is therefore not indicated in Fig. 1.

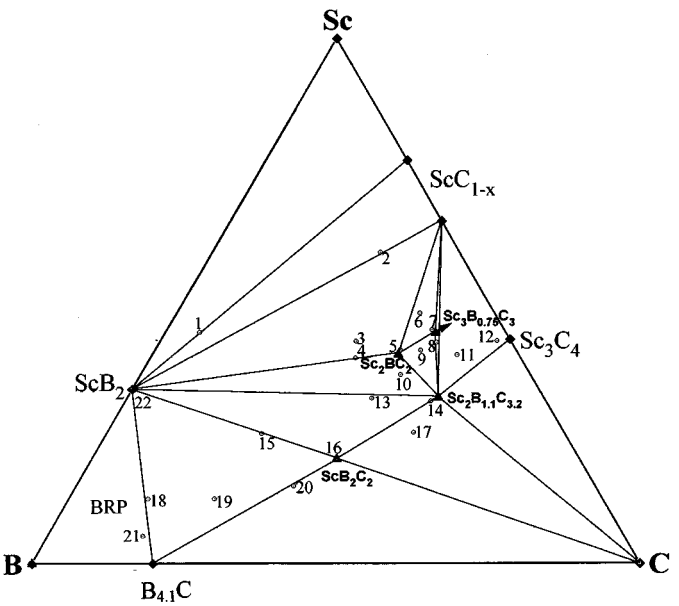

FIG. 1. Subsolidus phase relations in the system Sc–B–C. The phase region BRP (boron-rich part) denotes the boron rich (ScB_2–B–$B_{4.1}C$) section.

TABLE 2
Phase Analysis of the Boron Poor Sc–B–C Region

	Composition (Chemical analysis at.%)				Lattice parameters of hexagonal ScB_2 (Å)	
No.	Sc	B	C	Phase identification	*a*	*c*
1	44.24	50.25	5.50	$ScB_2 + ScC_{1-x}$	3.071(8)	3.530(9)
2	59.52	13.12	27.36	$ScC_{1-x} + ScB_2$	3.074(4)	3.525(5)
3	42.55	25.53	31.92	$Sc_2BC_2 + ScB_2 + ScC_{1-x}$	3.053(8)	3.531(8)
4	39.35	27.25	33.40	$Sc_2BC_2 + ScB_2$	3.052(6)	3.534(3)
5	40.90	19.18	39.92	Sc_2BC_2		
6	47.93	12.41	39.66	$ScC_{1-x} + Sc_2BC_2 + Sc_3B_{0.75}C_3$[a]		
7	44.69	11.99	43.32	$Sc_3B_{0.75}C_3$		
8	42.30	14.39	45.31	$ScC_{1-x} + Sc_3B_{0.75}C_3 + Sc_2B_{1.1}C_{3.2}$		
9	40.81	15.84	43.35	$Sc_3B_{0.75}C_3 + Sc_2BC_2 + Sc_2B_{1.1}C_{3.2}$		
10	36.17	21.52	42.31	$Sc_2BC_2 + Sc_2B_{1.1}C_{3.2} + ScB_2$	3.047(8)	3.551(9)
11	39.94	10.17	49.89	$Sc_2B_{1.1}C_{3.2} + ScC_{1-x} + Sc_3C_4$[a]		
12	42.54	2.27	55.18	$Sc_3C_4 + ScC_{1-x} + Sc_2B_{1.1}C_{3.2}$[a]		
13	31.65	28.48	39.87	$Sc_2B_{1.1}C_{3.2} + ScB_2$	3.0499(6)	3.5465(7)
14	31.10	18.97	49.92	$Sc_2B_{1.1}C_{3.2}$		
15	24.90	49.78	25.32	$ScB_2 + ScB_2C_2$	3.116(1)	3.518(2)
16	20.09	39.84	40.07	ScB_2C_2		
17	25.10	24.87	50.03	$Sc_2B_{1.1}C_{3.2} + ScB_2C_2 + C$		
18	12.38	74.56	13.06	$ScB_2 + B_4C$	3.149(3)	3.509(1)
19	12.41	63.74	23.85	$ScB_2 + B_4C + ScB_2C_2$	3.149(4)	3.511(2)
20	14.87	49.53	35.60	$ScB_2C_2 + B_4C$		
21	5.26	78.95	15.79	$ScB_2 + B_4C$	3.149(3)	3.514(3)
22	33.33	66.67	0	Pure ScB_2	3.1477(2)	3.5165(3)

[a]Phases only showing very weak peaks in the XRD patterns (→ minor amounts).

3.1.3. Boron Rich (ScB_2–B–$B_{4.1}C$) Section

In the ternary region (ScB_2–B–$B_{4.1}C$), at least three compounds "$ScB_{15}C_{0.80}$," $ScB_{15}C_{1.60}$, and $ScB_{17}C_{0.25}$ (6) (noted as I, II, and III in Fig. 2, respectively) were found. Figure 2 presents the phase diagram of the boron-rich part (BRP). The representative samples' chemical analysis results and phase identifications are listed in Table 3 and denoted in Fig. 2. All three ternary compounds are in equilibrium with B_4C. Our lattice parameter data (see Table 3), being

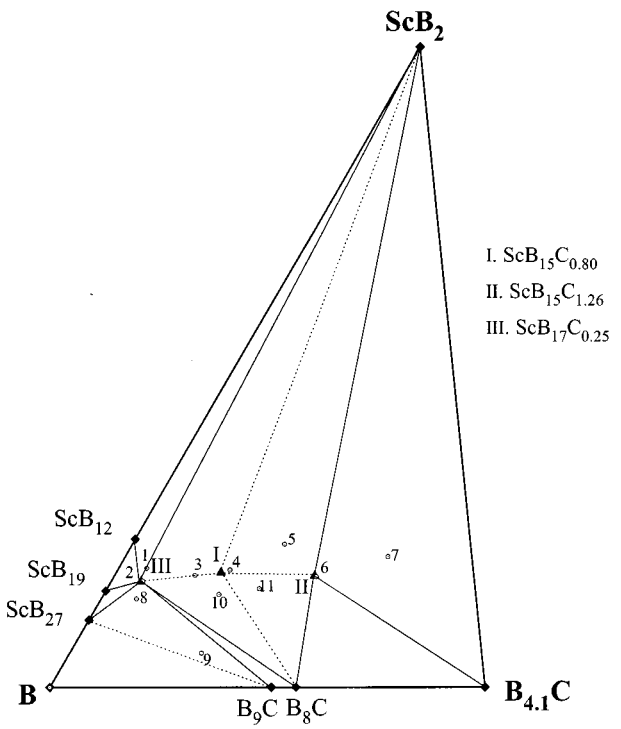

FIG. 2. Phase relations in the boron-rich (ScB_2–B–$B_{4.1}C$) section (BRP) (the dotted lines represent hypothetical equilibria).

basically in good accordance with previously found results for the composition range (16, 24), indicate no solubility of Sc in the B_4C lattice. The binary range of formation for B_4C was therefore accepted from literature data (24). As reported in (6), $ScB_{17}C_{0.25}$ has a wide homogeneity region from $ScB_{16}C_{0.20}$ to $ScB_{18.7}C_{0.64}$. For the sake of clarity for the whole diagram this phase is only represented by $ScB_{17}C_{0.25}$ in Fig. 2. The sample with the chemical analysis result $ScB_{15}C_{0.80}$ (noted as I in Fig. 2) showed the best XRD pattern with the fewest impurity phases. The oxygen content of this powder was 0.26 wt.%. Indexing has not been successful until now and neither has crystal growth. For this reason the hypothetical equilibria in this region are drawn with dotted lines.

TABLE 3
Phase Analysis of the Boron-Rich Sc–B–C Region

	Composition (Chemical analysis at.%)				Lattice parameters of boron carbide (Å)[b]	
No.	Sc	B	C	Phase identification	*a*	*c*
1	6.17	92.54	1.29	$ScB_{17.0}C_{0.25} + ScB_2$		
2	5.51	93.06	1.43	$ScB_{17.0}C_{0.25}$		
3	5.81	90.53	3.66	$ScB_{17.0}C_{0.25} + ScB_{15.0}C_{0.80}$		
4	6.08	88.81	5.11	$ScB_{15.0}C_{0.80}$[a]		
5	7.42	85.69	6.89	$ScB_{15.0}C_{1.60} + ScB_{15.0}C_{0.80} + ScB_2$		
6	5.73	85.12	9.14	$ScB_{15.0}C_{1.60} + ScB_2 + B_4C$		
7	6.78	81.36	11.86	$ScB_2 + B_4C + ScB_{15.0}C_{1.60}$	5.5997(6)	12.1151(2)
8	4.58	93.80	1.62	$ScB_{17.0}C_{0.25} + ScB_{27} + B_9C$	5.645(2)	12.229(5)
9	1.76	92.25	5.99	$ScB_{27} + B_9C$	5.643(2)	12.227(4)
10	4.81	89.94	5.25	$ScB_{17.0}C_{0.25} + ScB_{15.0}C_{0.80} + B_8C$	5.632(2)	12.210(3)
11	5.11	87.98	6.91	$ScB_{15.0}C_{1.60} + ScB_{15.0}C_{0.80} + B_8C$	5.634(2)	12.207(3)

[a]The XRD pattern of this sample is very complex; a small amount of ScB_2 and $ScB_{15.0}C_{1.60}$ can be found.
[b]Corresponds to hexagonal setting of B_4C.

3.2. Ternary Compounds

3.2.1. Crystal Growth and Structure Refinement of Sc_2BC_2

The existence and some structural details of Sc_2BC_2 were first mentioned in (42) and electronic structure calculations and a prediction of possible anisotropic transport properties were reported in Ref. (49), together with a graphical outline of the compound's unit cell. Reported lattice constants scatter (see Table 4). Since a congruent melting behavior was observed in Ref. (42) we made an attempt to grow crystals by the floating-zone method. The obtained crystal of a total length of 50 mm and 6 mm diameter was cut by spark erosion and metallographically analyzed. The grown specimen was found to contain three single crystalline grains. Pieces cut from one grain were examined on a Weissenberg

TABLE 4
Crystallographic Data of Sc_2BC_2

Crystal system	Tetragonal
Space group	$I4/mmm$
a (Å) (from powder data)	3.3259(2)
	3.330(1) (42)
	3.3 (49)
c (Å) (from powder data)	10.6741(8)
	10.659(2) (42)
	10.691 (49)
Volume (Å^3)	118.076(4)
Z	2
Formula weight	127.744
Calculated density (g/cm^3)	3.509
Applied radiation	Graphite monochrom. Mo$K\alpha$
Linear absorption coefficient μ (cm^{-1})	53.686
Crystal dimensions (mm)	$0.20 \times 0.15 \times 0.15$
Absorption correction	Gaussian numerical integration
Data corrections	Lorentz, polarization
Reflections measured	$0 \le h \le 7$, $-7 \le k \le 7$ $-24 \le l \le 24$
$2\theta_{max}$ (degree)	55
Total number of reflections	1646
Unique reflections	263
Structure solution, refinement programs	SIR92(51), SPD(15)
Number of variables	10
$R[F^2 > 2\sigma(F^2)]$	0.009
w$R(F^2)$	0.011
$(\Delta/\sigma)_{max}$	0.00

TABLE 5
Atomic Coordinates, Displacement Parameters, and Interatomic Distances for Sc_2BC_2

Atom	Site	X	Y	Z	U_{eq} (Å^2)	$U_{11} = U_{22}$ (Å^2)	U_{33} (Å^2)
Sc	4*e*	0	0	0.34759(1)	0.005(1)	0.004(1)	0.005(1)
C	4*e*	0	0	0.13816(4)	0.006(1)	0.005(1)	0.006(1)
B	2*a*	0	0	0	0.007(2)	0.007(1)	0.006(1)

Central atom	Ligands	Distance (Å)	Central atom	Ligands	Distance (Å)
Sc	1 C	2.2355(7)	C	1 B	1.4747(1)
	4 C	2.3567(2)		1 Sc	2.3555(7)
	4 B	2.8596(3)		4 Sc	2.3567(2)
	4 Sc	3.1418(4)	B	2 C	1.4747(1)
	1 Sc	3.2537(2)		8 Sc	2.8596(3)

Note. Refinement gave full occupancy of individual sites; the anisotropic displacement factor exponent takes the form $-2\pi^2(h^2a^{*2}U_{11} + \cdots + 2hka^*b^*U_{12})$, $U_{12} = U_{13} = U_{23} = 0$.

camera (Cu$K\alpha$ radiation). A tetragonal lattice showing no special extinctions beside the body centering conditions, $h + k + l = 2n + 1$, was confirmed. Details of single crystal data collection are given in Table 4. The results of the structure refinement are given in Table 5 together with bond distances. We confirm a structural model which can be derived from information found in (42, 49). The interatomic distances of Sc–Sc and Sc–C closely resemble distances found in the ScB_2C_2 compound (44). Rather, the contracted B–C distances of 1.4747(1) Å (1.484 Å in (49)) suggesting a strong double bond-like behavior in the short linear C–B–C chain are understood as the key features of this compound (50) (see Fig. 3).

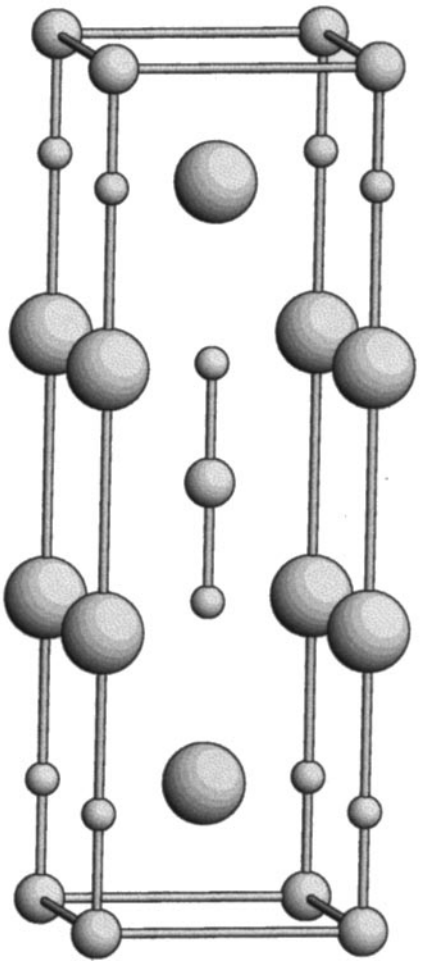

FIG. 3. A view of the Sc_2BC_2 structure. Large circles, Sc; medium, B; small, C.

3.2.2. *Ternary Compound $Sc_3B_{0.75}C_3$*

During the study of phase equilibria in the Sc-rich part of Sc–B–C a new phase was found at the nominal composition of $Sc_3B_{0.75}C_3$. The chemical analysis of several samples indicates the existence of a small homogeneity range: $Sc_3B_{0.75\pm x}C_{3+y}$ ($x \approx 0.03$, $0.02 < y < 0.1$) with oxygen content of 0.13 wt.%. The lattice parameters of the tetragonal primitive unit cell (see Table 6, no extinction rules observed) could be determined by the indexing program TREOR (46), i.e., $a = 3.3308(3)$ Å and $c = 7.680(2)$ Å with reliability merit value ($M(18) = 47$ and $F(18) = 17$). The crystal structure analysis and physical property measurement are currently undertaken and will be the subject of a different paper (35).

3.2.3. *Ternary Compound $Sc_2B_{1.1}C_{3.2}$*

Another new phase was synthesized near the nominal composition of $Sc_2B_{1.1}C_{3.2}$. The chemical analysis of the nearly single-phase sample showed its composition as $Sc_2B_{1.11}C_{3.24}$ with oxygen content of about 0.80 wt.%. The lattice parameters of the unit cell could be determined with trigonal or hexagonal symmetry by the indexing program TREOR (46), i.e., $a = b = 3.3991(2)$ Å and $c = 6.7140(6)$ Å with high merit value ($M(19) = 111$ and $F(19) = 40$). Nevertheless some unidentified weak peaks (no binary or ternary impurity!) could not be indexed based on this small unit cell.

Figure 4 shows the morphology of layered platelets of the as-prepared compound $Sc_2B_{1.1}C_{3.2}$ observed by scanning electron microscopy. Because of this layer property the compound shows a strong tendency of preferred cleavage resulting in crystal sheets parallel to (001). Therefore an electron diffraction pattern (EDP) with the electron beam parallel to the [100] axis could not be achieved. The EDP in the a^*–b^* plane is shown in Fig. 5. A careful analysis revealed that the positions of the intense spots in the EDP form the basic hexagonal or trigonal structure and the weak

TABLE 6
Powder X-Ray Diffraction Data of $Sc_3B_{0.75}C_3$

h	k	l	d_{obs}	d_{cal}	I_{obs}
0	0	1	7.68	7.68	9
0	0	2	3.839	3.840	6
1	0	0	3.336	3.331	3
1	0	1	3.056	3.056	10
0	0	3	2.560	2.560	25
1	0	2	2.517	2.516	33
1	1	0	2.356	2.355	100
1	1	2	2.008	2.008	3
0	0	4	1.9194	1.9199	10
1	1	3	1.7342	1.7333	12
2	0	0	1.6654	1.6654	17
1	1	4	1.4874	1.4881	6
2	1	1	1.4618	1.4623	3
2	0	3	1.3956	1.3960	9
1	0	5		1.3948	
2	1	2	1.3890	1.3888	17
2	0	4	1.2585	1.2581	3
2	2	0	1.1781	1.1776	5
3	2	2	0.8980	0.8982	3

Note. The d values are given in Å.

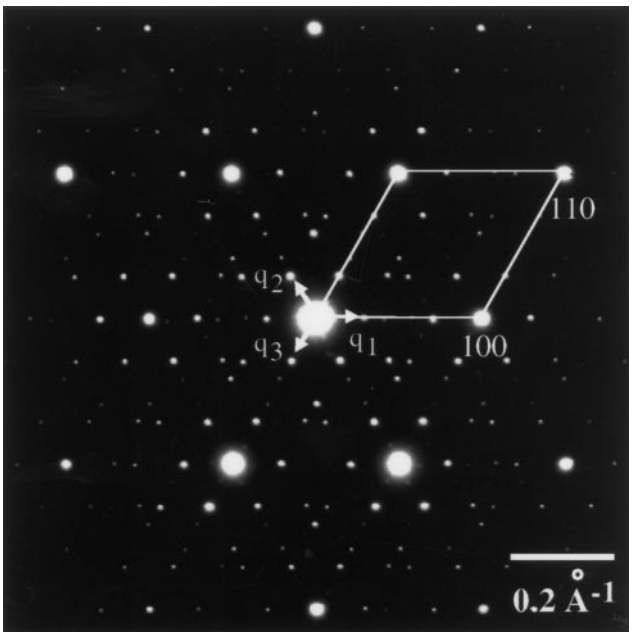

FIG. 5. Electron diffraction patterns of the $Sc_2B_{1.1}C_{3.2}$ compound with the electron beam parallel to the [001] axis. Indices are based on the hexagonal subcell.

spots can be explained by assuming an incommensurate structure. Figure 6 schematically shows the position of diffraction spots expected by this assumption. The triple waves $q_i = (i = 1, 2, 3)$ (one of which is indicated as A) have the incommensurate vectors along [100] directions with magnitude $|q_i| = (2/7 + 0.005)\,|q_{100}|$ Å^{-1}, where q_{100} is the wave vector for the basic spot. Satellite spots indicated as B and C correspond to the second-order incommensurate waves of $2\,q_1$ or q_1–q_2 type, respectively. The spots D correspond to the third-order incommensurate wave of $3q_1$ type. If the a and b lattice parameters are expanded to seven times the basic unit cell, i.e., $a = b = 23.84(2)$ Å and $c = 6.710(9)$ Å, all the peaks in the XRD pattern of the powder sample

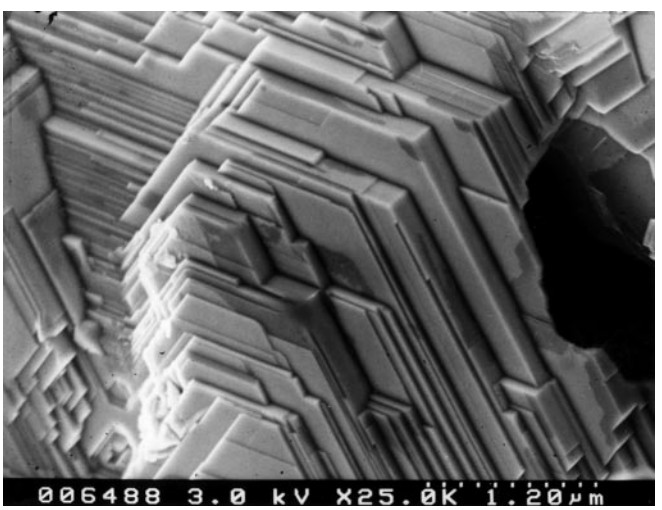

FIG. 4. Scanning electron microscopy photograph of as-prepared $Sc_2B_{1.1}C_{3.2}$.

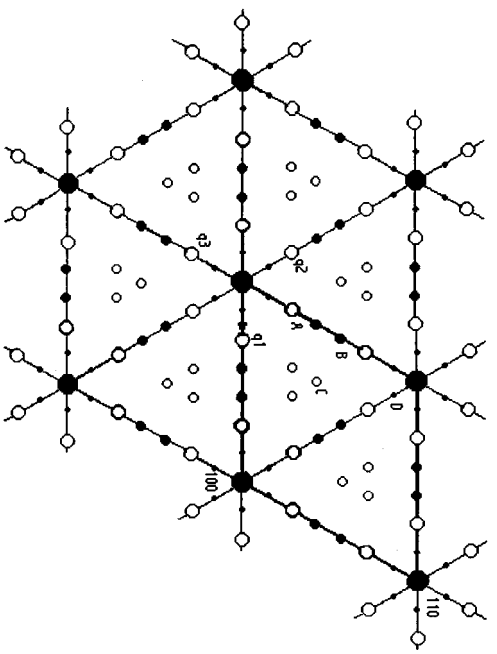

FIG. 6. Schematic representation of the EDP from a modulated layer corresponding to Fig. 5. Large solid circles represent the basic spots and the medium open circles the first-order satellite spots indicated as A. Small solid and open circles indicated as B and C represent the second-order satellite spots. The smallest solid circles denoted as D correspond to the third-order satellite spots.

TABLE 7
Powder X-Ray Diffraction Data of $Sc_2B_{1.1}C_{3.2}$

h	k	l^a	h	k	l^b	d_{obs}	d_{cal}	I_{obs}
0	0	1	0	0	1	6.68	6.71	26
0	0	2	0	0	2	3.356	3.355	4
7	0	0	1	0	0	2.947	2.949	17
7	0	1	1	0	1	2.670	2.670	100
5	0	2				2.608[c]	2.606	2
5	1	2				2.501[c]	2.499	3
5	2	2				2.357[c]	2.354	4
0	0	3	0	0	3	2.237	2.237	61
7	0	2	1	0	2	2.215	2.215	70
2	0	3				2.184[c]	2.186	10
9	0	1				2.164[c]	2.170	7
5	2	3				1.8542[c]	1.8523	2
7	0	3	1	0	3	1.7823	1.7820	19
4	5	3				1.7075[c]	1.7073	24
7	7	0	1	1	0	1.7028	1.7025	18
7	7	1	1	1	1	1.6502	1.6502	7
7	7	2	1	1	2	1.5183	1.5182	5
7	0	4	1	0	4	1.4582	1.4580	12
14	0	1	2	0	1	1.4400	1.4401	8
7	7	3	1	1	3	1.3547	1.3547	8
14	0	2	2	0	2	1.3500	1.3498	8
0	0	5	0	0	5	1.3415	1.3419	4
14	0	3	2	0	3	1.2213	1.2310	4

Note. The d values are given in Å.
[a]The indexing results based on seven times the small unit cell.
[b]The indexing results of the basic unit cell.
[c]The peaks which cannot be indexed by small basic lattice parameters.

could be indexed. The indexing results on the basis of both the small unit cell and the one seven times larger are given in Table 7. A small single crystal of $Sc_2B_{1.1}C_{3.2}$ has been obtained by the floating-zone method. The crystal structure analysis is in progress and is the subject of a different paper (48).

3.2.4. *Boron-Rich Compound $ScB_{15}C_{1.60}$*

As mentioned in (6), another unknown ternary phase was found near $ScB_{17}C_{0.25}$. During the phase diagram determination it was recognized that this new phase exists in the region of $ScB_{15}C_x$ ($1.0 < x < 2.0$). A composition of $ScB_{15}C_{1.60}$ (oxygen impurity content of 0.23 wt.%) was found to represent this new compound (noted as II in Fig. 2). X-ray powder diffraction data are presented in Table 8 together with the observed and calculated interplanar d-spacings. EDP of the a^*–b^* and a^*–c^* planes are shown in Figs. 7a and 7b. The hkl assignments for both X-ray diffraction peaks and electron diffraction spots were carried out according to an orthorhombic cell with $a = 10.027(1)$ Å, $b = 8.0138(9)$ Å, $c = 5.6668(6)$ Å, and $V = 455.352(2)$ Å^3. The extinction condition $h + k + l = 2n + 1$ for a body centered lattice obtained from both the electron diffraction patterns and the full indexing of the X-ray diffraction peaks indicate that the possible space groups of this structure are $Immm$, $I222$, $I2_12_12_1$, and $Imm2$.

A polycrystalline pellet was arc-melted in order to investigate the melting property of this compound. After arc-melting it was found to decompose to ScB_2, ScB_{12}, and B_4C. This result indicates that $ScB_{15}C_{1.60}$ decomposes without melting and cannot be conventionally grown from a melt phase.

TABLE 8
Powder X-Ray Diffraction Data of $ScB_{15}C_{1.60}$

h	k	l	d_{obs}	d_{cal}	I_{obs}
1	1	0	6.28	6.26	35
2	0	0	5.02	5.01	3
0	1	1	4.63	4.63	7
0	2	0	4.01	4.01	14
2	1	1	3.404	3.400	100
1	2	1	3.112	3.110	25
3	1	0	3.087	3.084	29
0	0	2	2.836	2.833	28
1	1	2	2.583	2.581	11
1	3	0		2.581	
2	0	2	2.469	2.467	90
0	3	1	2.417	2.416	10
3	2	1	2.339	2.338	53
0	2	2	2.316	2.313	4
4	1	1	2.205	2.204	24
2	3	1	2.177	2.177	72
4	2	0	2.124	2.125	3
2	2	2	2.101	2.101	8
3	1	2	2.088	2.087	54
3	3	0		2.088	
0	4	0	2.004	2.003	13
5	1	0	1.9458	1.9454	19
1	3	2	1.9088	1.9082	19
2	4	0	1.8610	1.8604	7
0	1	3	1.8392	1.8386	5
4	3	1	1.7397	1.7397	5
5	2	1	1.7096	1.7098	18
1	2	3	1.6852	1.6843	11
6	0	0	1.6710	1.6712	10
0	4	2	1.6359	1.6358	8
5	1	2	1.6040	1.6038	7
4	4	0	1.5647	1.5650	5
2	4	2	1.5552	1.5551	9
6	2	0	1.5424	1.5424	23
4	1	3	1.4827	1.4826	5
2	5	1	1.4742	1.4741	8
0	0	4	1.4170	1.4167	9
5	3	2	1.3956	1.3957	6
7	2	1	1.3121	1.3122	12
5	2	3	1.3005	1.3006	15
3	5	2	1.2874	1.2874	22
5	5	0	1.2520	1.2520	7
3	6	1	1.2115	1.2116	5

Note. The d values are given in Å.

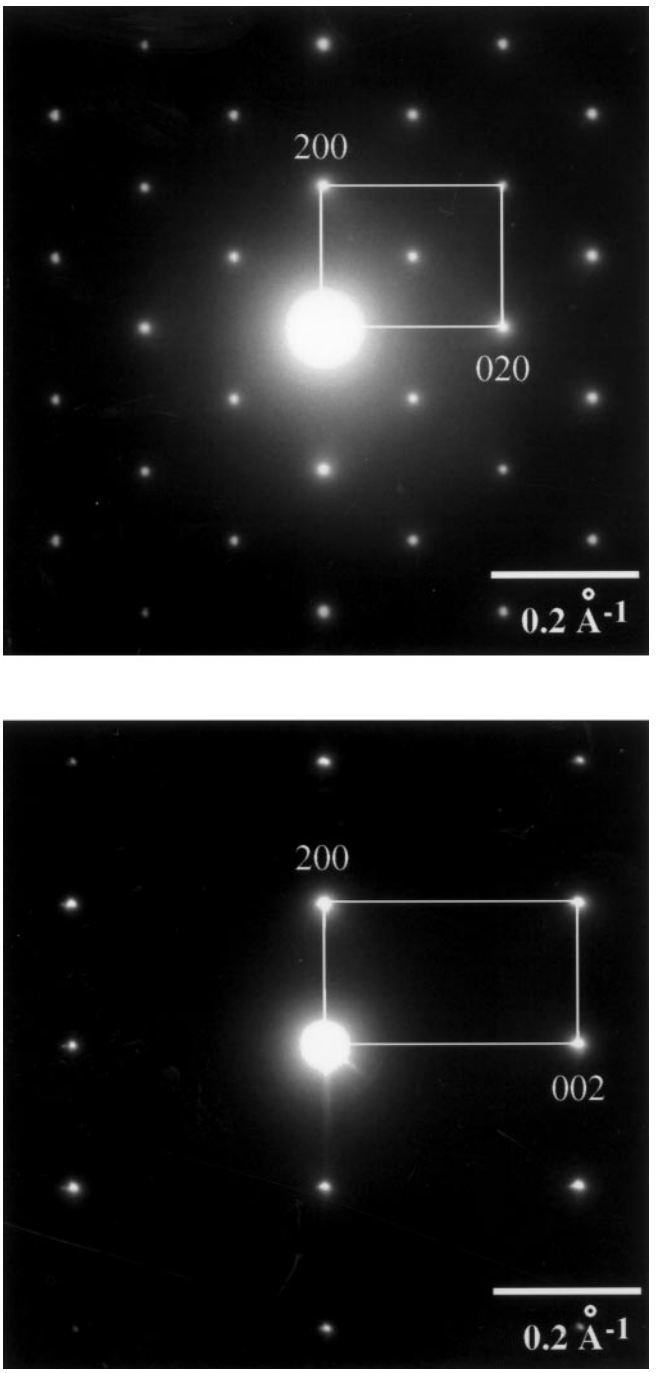

FIG. 7. Electron diffraction patterns of $ScB_{15}C_{1.60}$ compound in (a) a^*–b^* and (b) a^*–c^*.

4. CONCLUSIONS

The phase equilibria in the ternary system scandium–boron–carbon have been established with an isothermal section at 1700°C. The combined approach of solid state powder metallurgical techniques and floating-zone crystal growth has been successfully applied to the synthesis and analysis of boro-carbide-based materials. Four novel ternary compounds, $Sc_3B_{0.75}C_3$, $Sc_2B_{1.1}C_{3.2}$, $ScB_{15}C_{1.60}$, and $ScB_{15}C_{0.8}$, were identified. The crystal structure of Sc_2BC_2 was refined from single crystal data. Oxygen impurity content was monitored throughout usually lying below 1 wt.% in the ternary and was found to show only influence on the structural characteristics of the binary ScC_{1-x} phase. The boron-rich compounds merit further exploration with regard to development of crystal growth techniques.

ACKNOWLEDGMENTS

Ying Shi is grateful for STA fellowship. The authors thank Mr. A. Sato for carrying out the four-circle analysis and useful discussion. They are also indebted to Dr. M. Uchida, Mr. Y. Kitami, Mr. M. Tutumi, Mr. S. Takenouchi, and Mr. Y. Yajima for electron diffraction, scanning electron microcopy, and chemical analysis, respectively.

REFERENCES

1. J. Bauer and H. Nowotny, *Monatsh. Chem.* **102,** 1129 (1971).
2. K. A. Schwetz, M. Hörle, and J. Bauer, *Ceram. Int.* **5**(3), 105 (1979).
3. P. K. Smith and P. W. Gilles, *J. Inorg. Nucl. Chem.* **29,** 375 (1967).
4. J. Bauer, P. Vennegues, and J. L. Vergneau, *J. Less-Common Met.* **110,** 295 (1985).
5. P. Rogl, *in* "Phase Diagrams of the Ternary Metal–Boron–Carbon Systems" (G. Effenberg, Ed.). ASM International, 1998.
6. T. Tanaka, *J. Alloys Comp.* **270,** 132 (1998).
7. G. Y. Adachi, N. Imanaka, and F. Z. Zhang, *in* "Handbook on the Physics and Chemistry of Rare-earths" (K. A. Gschneidner and L. Eyring, Eds.), Vol. 15, p. 115, Elsevier, Amsterdam/New York, 1991.
8. G. S. Smith, Q. Johnson, and P. C. Nordine, *Acta Cryst.* **19,** 668 (1965).
9. J. Wong, G. N. George, I. J. Pickering, Z. U. Rek, M. Rowen, T. Tanaka, G. H. Via, B. DeVries, D. E. W. Vaughan, and G. E. Brown Jr., *Solid State Commun.* **92,** 559 (1994).
10. T. Tanaka, S. Okada, and Y. Ishizawa, *J. Alloys Comp.* **205,** 281 (1994).
11. T. Tanaka, S. Okada, Y. Yu, and Y. Ishizawa, *J. Solid State Chem.* **133,** 122 (1997).
12. T. Tanaka, S. Okada, and V. N. Gurin, *J. Alloys Comp.* **267,** 211 (1998).
13. T. Tanaka, S. Okada, and Y. Ishizawa, *J. Solid State Chem.* **133,** 55 (1997).
14. B. Hájek, P. Karen, and V. Brozek, *J. Less-Common Met.* **99,** 245 (1984).
15. B. A. Frenz and Associates, "SDP for Windows Reference Manual." College Station, TX, 1995.
16. F. Thevenot, *J. Eur. Ceram. Soc.* **6,** 205 (1990).
17. B. Kasper, Thesis, MPI-PML, Stuttgart, Germany, 1996.
18. H. K. Clarke and J. L. Hoard, *J. Am. Chem. Soc.* **65,** 2115 (1943).
19. B. Morosin, T. Aselage, and R. Feigelson, *in* "Novel Refractory Semiconductors" (D. Emin, T. L. Aselage, and C. Wood, Eds.), p. 70. Amer. Inst. Phys., NY, 1986.
20. T. L. Asalage and R. G. Tissot, *J. Am. Cream. Soc.* **75,** 2207 (1992).
21. G. H. Kwei and B. Morosin, *J. Phys. Chem.* **100,** 8031 (1996).
22. V. H. Neidhard, R. Mattes, and H. J. Becher, *Acta Crystallogr. B* **26,** 315 (1970).
23. U. Kuhlmann, H. Werheit, and K. A. Schwetz, *J. Alloys Comp.* **189,** 249 (1992).
24. M. Bouchacourt and F. Thevenot, *J. Less-Common Met.* **82,** 219 (1981).
25. T. B. Massalski, "Binary Alloy Phase Diagrams," 2nd ed. ASM International, 1990.

26. B. Callmer, *J. Solid State Chem.* **23,** 391 (1978).
27. V. A. Bruskov, L. V. Zavalii, and Yu. B. Kuz'ma, *Inorg. Mater.* (Izv. Akad. Nauk SSSR, Neorg. Mater.) **24,** 420 (1988).
28. V. I. Matkovich, J. Economy, R. F. Giese Jr., and R. Barret, *Acta Cryst.* **19,** 1056 (1965).
29. Y. Paderno and N. Shitsevalova, *J. Alloys Comp.* **219,** 119 (1995).
30. A. Leithe-Jasper and T. Tanaka, *in* "Proceedings 43rd Symposium of Synthetic Crystals," Osaka, Japan, 11–13 Nov. 1998, paper 2A1, p. 69.
31. T. Ya. Velikanova, V. N. Eremenko, L. V. Artyukh, A. A. Bondar, and O. V. Gordiichuk, *Sov. Powder Metall. Met. Ceram.* **28,** 711 (1989).
32. H. Rassaerts, H. Nowotny, G. Vinek, and F. Benesovsky, *Monatsh. Chem.* **98,** 460 (1967).
33. H. Auer-Welsbach and H. Nowotny, *Monatsh. Chem.* **92,** 198 (1961).
34. H. Nowotny and H. Auer-Welsbach, *Monatsh. Chem.* **92,** 789 (1961).
35. N. H. Krikorian, A. L. Bowman, M. C. Krupka, and G. P. Arnold, *High Temp. Sci.* **1,** 360 (1969).
36. B. Hájek, P. Karen, and V. Brozek, *J. Less-Common Met.* **96,** 35 (1984).
37. H. Nowotny and A. Neckel, *J. Inst. Met.* **97,** 161 (1969).
38. B. Hajek, P. Karen, V. Brozek, *Monatsh. Chem.* **117,** 1271 (1986).
39. M. Atoji and M. Kikuchi, *J. Chem. Phys.* **51,** 3863 (1969).
40. H. Jedlicka, H. Nowotny, and F. Benesovsky, *Monatsh. Chem.* **102,** 1129 (1971).
41. R. Pöttgen and W. Jeitschko, *Inorg. Chem.* **30,** 427 (1991).
42. J. Bauer, M. Potel, P. Gougeon, J. Padiou and H. Noël, *in* "Proc. 9th Int. Conf. on Solid Compounds of Transition Elements," Royal Society of Chemistry, Dalton Division, 4–8 July, 1988, Oxford.
43. J. Bauer, *J. Less-Common Met.* **87,** 45 (1982).
44. G. S. Smith, Q. Johnson, and P. C. Nordine, *Acta Crystllogr.* **19,** 668 (1965).
45. P. Peshev, J. Etourneau, and R. Naslain, *Mater. Res. Bull.* **5,** 319 (1970).
46. P. E. Werner, L. Eriksson, and M. Westdahl, *J. Appl. Crystallogr.* **23,** 292 (1990).
47. Ying Shi, A Leithe-Jasper, and T. Tanaka, *J. Alloy Comp.*, in press.
48. Y. Shi, A Leithe-Jasper, L. Bourgeois, Y. Bando, and T. Tanaka, *J. Solid State Chem.*, in press.
49. J.-F. Halet, J.-Y. Saillard, and J. Bauer, *J. Less-Common Met.* **158,** 239 (1990).
50. J. Bauer, G. Boucekkine, G. Frapper, J.-F. Halet, J.-Y. Saillard, and B. Zouchoune, *J. Solid State Chem.* **133,** 190 (1997).
51. A. Altomare, G. Cascarano, C. Giacovazzo, A. Guagliardi, M. C. Burla, G. Polidori, and M. Camalli, *J. Appl. Crystallogr.* **27,** 435 (1994).